Investigation of the Effect of 475 °C Aging Treatment on Mechanical Properties of a Fe–19Cr–5.5Al ODS Alloy Using Tensile, Impact and Small Punch Tests

Andrea García-Junceda, Diego Rodríguez, Rebeca Hernández & Marta Serrano

Abstract

The effect of thermal aging on the mechanical properties of a Fe–19Cr–5.5Al oxide dispersion strengthened (ODS) hot rolled steel plate was evaluated. Tensile tests, sub-size Charpy impact tests, microhardness measurements and small punch tests were performed to analyze the embrittlement phenomenon occurring at an aging temperature of 475 °C as a consequence of a miscibility gap in the Fe–Cr system. These mechanical tests were able to confirm the age hardening and its intensity grade at different testing temperatures. Fractured impact and small punch specimens exhibited parallel delaminations promoted by a microstructure formed by elongated ferritic grains with a texture being 〈110〉 along the rolling direction. This study has revealed that small punch test represents a valuable technique for assessing the embrittlement susceptibility of high-Cr ODS alloys at different operational temperatures.

1 Introduction

Oxide dispersion strengthened (ODS) ferritic steels are structural materials proposed for the IV generation of fission nuclear reactors and advanced fusion reactors. They are excellent candidates as nuclear materials due to their good resistance to both creep and neutron irradiation embrittlement. These outstanding properties are mainly due to a fine-grained microstructure and the presence of highly stable nanosized oxide particles acting as sinks for radiation-induced defects such as vacancies and interstitials.[1,2,3,4] The combined addition of a Cr content superior to 13 wt pct and an Al content around 5 wt pct has been reported to be an effective way to highly suppress the corrosion of ODS steels, which is of special interest for these alloys since they are proposed to work during long-term harsh operational conditions.[5,6] However, the high-Cr content may lead to the undesirable so-called “475 °C embrittlement” due to long time exposure of steels at this high temperature [7] or caused by crossing the 475 °C range at the beginning and end of operation cycles in nuclear reactors. The embrittlement is typical of ferritic alloys in which a Fe-rich phase (α) and a Cr-rich phase (α') are formed due to the existence of a miscibility gap, existing below approximately 500 °C in the Fe–Cr binary equilibrium system.[8,9] This phenomenon reaches particular importance in ODS materials, in which the working service temperatures could lie in the range of 300 °C to 550 °C. Capdevila *et al*. analyzed the phase separation between α and α' by atom probe tomography in a hot rolled PM2000 steel tube, with nominal composition Fe–19Cr–5.5Al–0.5Ti–0.5Y_2O_3 (in wt pct), and determined that the nanometric-scaled

phase separation was the main mechanism producing a hardness increase during aging at 475 °C [10,11], probably due to the limitation in the glide of the dislocations attending to the studies of Terentyev et al.[12] This phase separation resulted in the formation of isolated particles of chromium-enriched α' phase with a size around 5 to 10 nm after 100 hours of aging treatment. Degmová *et al.* confirmed the formation of bcc Cr-rich precipitates in PM2000 steel with aging time at 475 °C using Mössbauer spectroscopy.[13] The increase in hardness led to an embrittlement of the alloy, which was related to be linearly dependent on the content of chromium in the α' regions.[10] According to Capdevila *et al.* this hardening effect seemed to be saturated after an aging of 1000 hours at 475 °C.[11] More recently, Maji *et al.* found that the hardness values of spark plasma sintered FeCrAl ODS alloys, with Cr and Al contents between 12 to 22 and 8 to 16 wt pct, respectively, reached to their maxima after 100 hours aging at 475 °C, irrespective of their Al contents.[14] The hardness achieved remained more or less constant during a total aging time of 1000 hours. Supporting the fact of the embrittlement at 475 °C, delaminations were reported by Chao *et al.* to severely occur during tensile testing of a hot rolled PM2000 tube.[15] However, these authors did not performed impact or small punch tests in the PM2000 tube to determine the age hardening susceptibility of this high-Cr ODS alloy.

To further analyze the 475 °C thermal aging effect on the mechanical properties of a high-Cr steel, in the present study a hot rolled PM2000 plate alloy was mechanically tested in both as-received and aged conditions by means of tensile, Charpy impact and small punch tests. The experimental curves and fractured specimens obtained from these tests were analyzed to evaluate the level of hardening introduced by the aging treatment. In addition, the paper aims at comparing the results obtained by these different mechanical testing techniques to assess if small punch testing could be a suitable technique to determine the embrittlement grade of an aged hot rolled alloy.

2 Experimental Procedure

The chemical composition (wt pct) of the PM2000 plate supplied by Plansee Group is Fe–19Cr–5.5Al–0.5Ti–0.5Y_2O_3. This alloy is formed by ferritic grains containing approximately 0.5 wt pct of fine, uniformly dispersed, yttrium oxide particles.[16] The ODS steel was mechanically alloyed, followed by hot extrusion and hot rolling. The final size was 30 × 26 × 1300 mm^3. The aging treatment was performed in a horizontal tubular furnace at 475 °C during 1000 hours in Ar atmosphere. Hot rolled and aged samples were ground and polished by standardized methods for metallographic examination in LT, LS and TS orientations. The microstructural characterization was performed with a Field Emission Gun Microscope (FEG-Helios Nanolab 600i FEI) coupled to Electron Backscatter Diffraction (EBSD-Oxford Instruments HKL NordlysNano detector). The acquisitions were conducted at an accelerating voltage of 15 kV, a beam current of 5.5 nA with a step size equal to 0.04 μm. The microtexture analysis were performed using the Inverse Pole Figure maps (IPF-EBSD) by selecting grain boundaries with misorientation angles above 5 deg and using an analysis software package Channel 5.0 for the acquisition. These IPF maps were also used for the calculation of the average ferritic grain size and the Grain Aspect Ratio (GAR).

Tensile tests were carried out at room temperature in an MTS universal machine with a 100 kN load cell on as-received and aged M10 L-Tensile specimens. These tests were done under stroke control at a displacement rate of 0.1 mm/min (corresponding to a strain of 1×10^{-4} s^{-1}). Impact tests were performed on a small-scaled instrumented Charpy machine of 25 J capacity at a velocity of 3.85 m/s. Miniaturized V-notch specimens with KLST geometry ($4 \times 3 \times 27$ mm^3) were machined in the longitudinal orientation (LT) and tested at temperatures between − 130 °C and 202 °C. The ductile-to-brittle transition temperature (DBTT) was calculated as the temperature at which the absorbed energy is equal to one-half of the sum of the upper and the lower shelf energies (USE and LSE, respectively). With the aim of evaluating the microhardness in the different orientations of the ODS plate, samples were subjected to a load of 0.1 kg for 10 seconds using a Vickers hardness testing machine. The hardness test was repeated ten times for each orientation in order to calculate and average value. Small punch tests were carried out in disk samples with 6 mm diameter and 0.5 mm thick, manufactured by electro-discharge machining in the rolling direction of the plate, corresponding to the mechanical behavior of the TS plane, and followed by a slight grinding with 1200 sand paper. As-received and aged samples were tested at 24 °C, 100 °C, 200 °C and 475 °C with a punch tip diameter of 2.5 mm and at a rate displacement of 0.3 mm min^{-1}, following the Standard Test Method for Small Punch Testing of Metallic Materials.[17] The longitudinal orientation was selected for impact, small punch and tensile test specimens due to the geometry of the plate, which did not allow to test in other orientations. Figure 1 shows schematically all the planes found in the steel plate with the corresponding orientation of the Charpy impact, small punch and tensile specimens tested.

Fig. 1

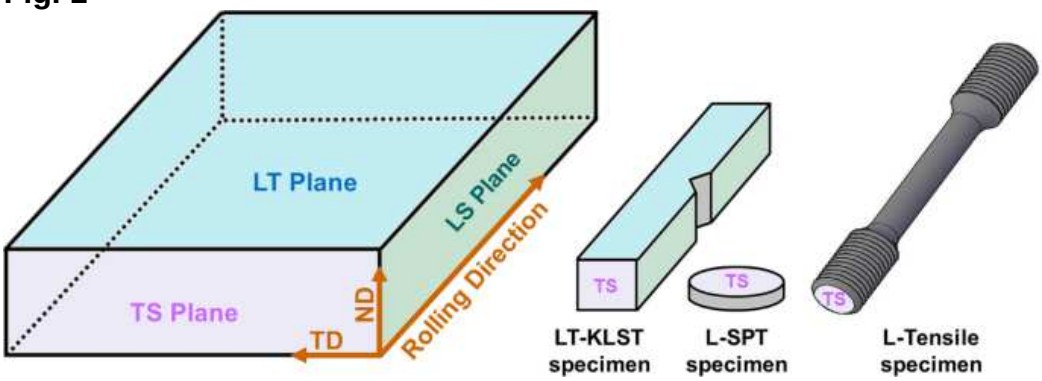

Scheme with the sections of the planes analyzed by EBSD and the orientation of the impact, small punch and tensile specimens

3 Experimental Results and Discussion

3.1 Microstructural Characterization

The study of the microstructure was performed on the three orientations of the steel plate (LS, TS and LT) for both as-received and aged ODS alloy. As expected, the IPF maps in Figures 2 and 3 show a fine microstructure formed by elongated ferritic grains (GAR= 2.5 ± 0.2) in the rolling direction (LS plane) with an average diameter grain size of 0.9 ± 0.1 μm. The average grain size in the TS plane is slightly smaller, 0.7 ± 0.1 μm,

although the grains are also elongated (GAR= 2.7 ± 0.2), whereas in the LT plane the grains are more equiaxed (GAR= 1.7 ± 0.1) with an average grain size of 0.9 ± 0.1 μm. The size of the grains does not vary significantly with the aging treatment in any of the orientations studied. These maps acquired by EBSD reflect the texture presented in the sample in two main directions (RD and ND) and they highlight two strong preferential crystallographic orientations of the grains, being 〈110〉 along the rolling direction (Figure 2) and 〈100〉 along the normal direction of the plate (Figure 3). These crystallographic orientations do not seem to be affected by the aging treatment at 475 °C during 1000 hours. In addition, the analysis of the Orientation Distribution Function (ODF) maps acquired at $\varphi 2 = 45$ deg section of Euler space clarifies the main texture components found in this rolled alloy.[18] A typical dominating texture component (110)〈110〉 of ferritic alloys is present in the LS and TS orientations. On the other hand, the components (001)〈110〉 are visible in the LT orientation (Figure 4).

Fig. 2

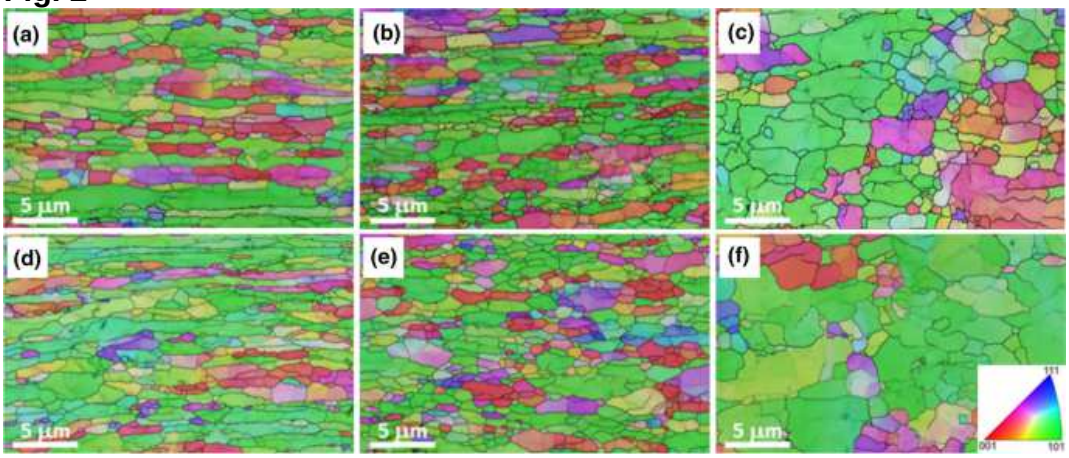

IPF-EBSD maps showing a preferential crystallographic orientation of the grains being 〈110〉 along the RD corresponding to the planes: (*a*) LS as-received, (*b*) TS as-received, (*c*) LT as-received, (*d*) LS aged, (*e*) TS aged and (*f*) LT aged

Fig. 3

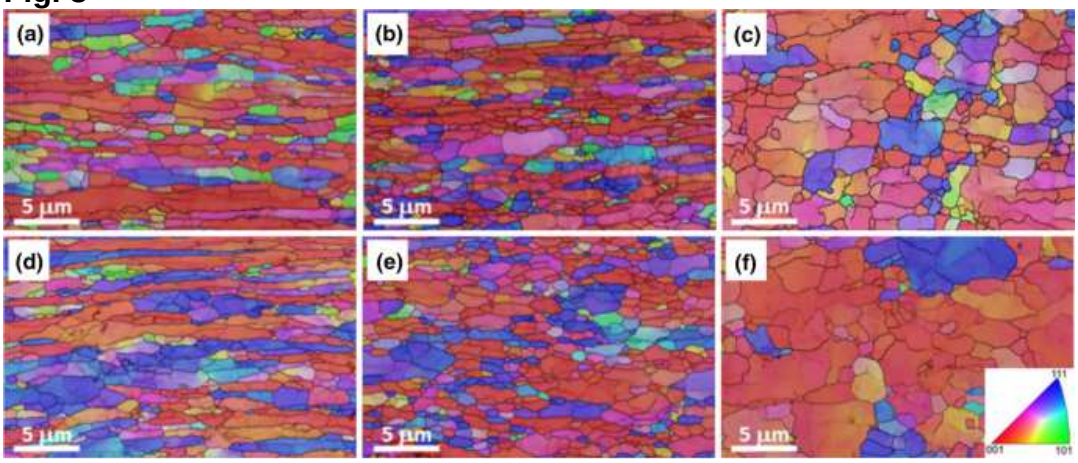

IPF-EBSD maps showing a preferential crystallographic orientation of the grains being 〈100〉 along the ND corresponding to the planes: (*a*) LS as-received, (*b*) TS as-received, (*c*) LT as-received, (*d*) LS aged, (*e*) TS aged and (*f*) LT aged

Fig. 4

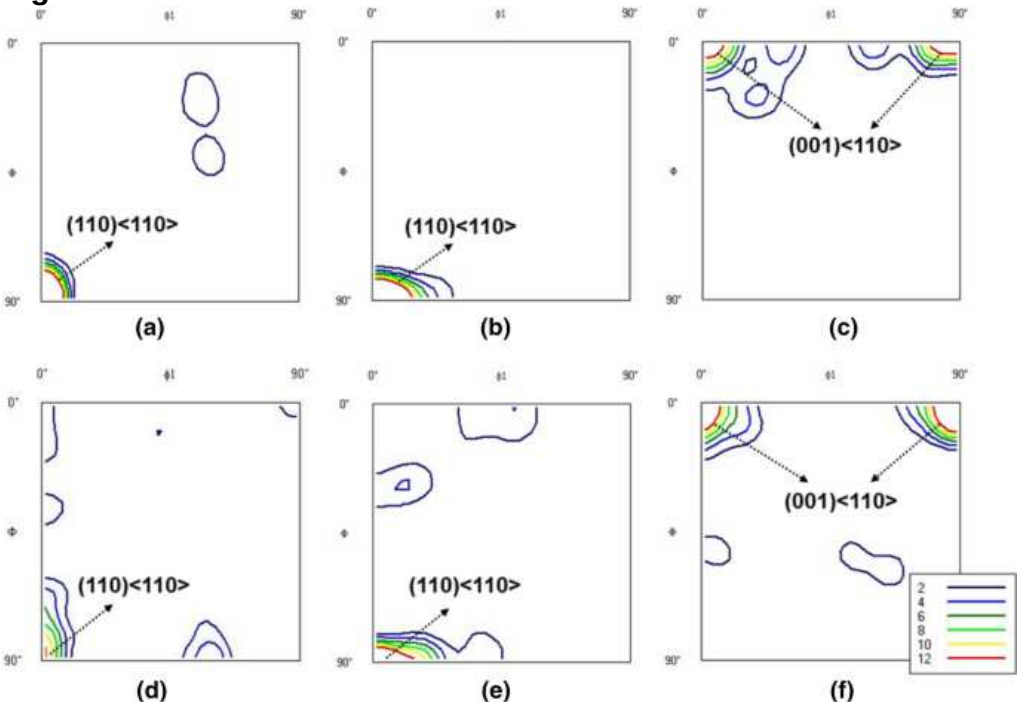

ODF maps at $\varphi 2$ = 45 deg section of Euler space showing the body centered cubic (bcc) texture components corresponding to the planes: (*a*) LS as-received, (*b*) TS as-received, (*c*) LT as-received, (*d*) LS aged, (*e*) TS aged and (*f*) LT aged

3.2 Tensile Tests

To analyze the effect of the aging treatment on stress–strain behavior of the PM2000 plate, tensile tests were performed at room temperature as a first approach. From the curves shown in Figure 5 it is noticeable that the aging produces an slight increase of the yield strength, a significant increase in the ultimate tensile strength (UTS) from 1038 to 1341 MPa, together with a drop of ductility from 15.5 to 10.5 pct. The increase of both the yield strength and UTS after the aging treatment can be related to the formation of the nanometric Cr-rich α' phase, since this phase is acting as additional obstacle to the movement of dislocations increasing the strength of the ODS alloy. These facts clearly suggest an embrittlement induced by the treatment at 475 °C during 1000 hours, which is also perceptible in the fracture images of the tensile specimens. In the case of the aged fractured specimen, a more brittle fracture with the presence of delaminations is observable.

Fig. 5

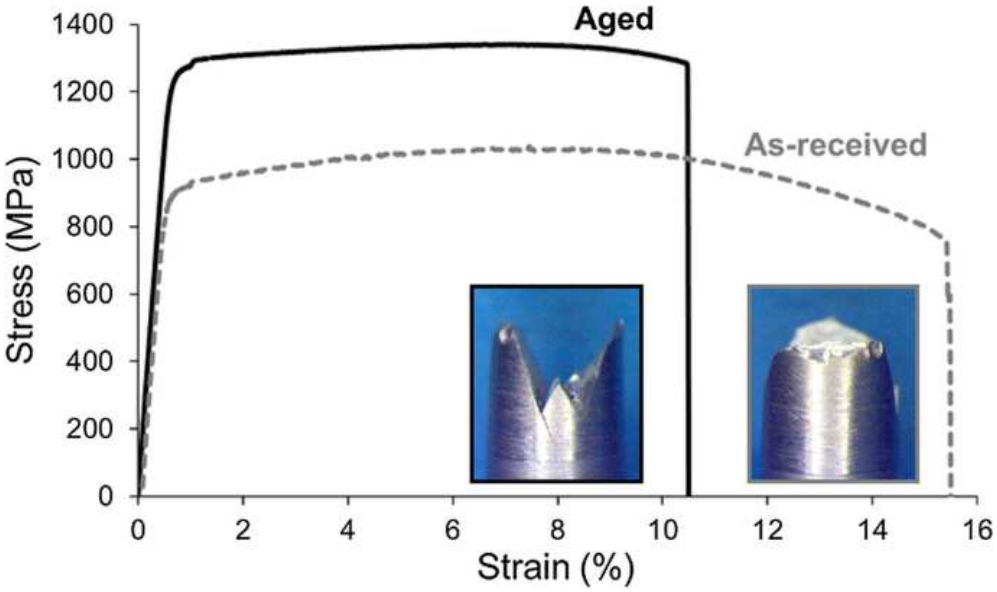

Engineering tensile stress-strain curves obtained at room temperature from tensile tests on as-received and aged conditions in the Fe–19Cr–5.5Al ODS alloy

3.3 Sub-size Charpy Impact Tests and Vickers Microhardness

The plot showing the absorbed impact energies achieved against the testing temperature for both as-received and aged alloys is shown in Figure 6. From these experimental curves, it is obvious that the aging treatment leads to a decrease in the impact absorbed energy for a given testing temperature.

Fig. 6

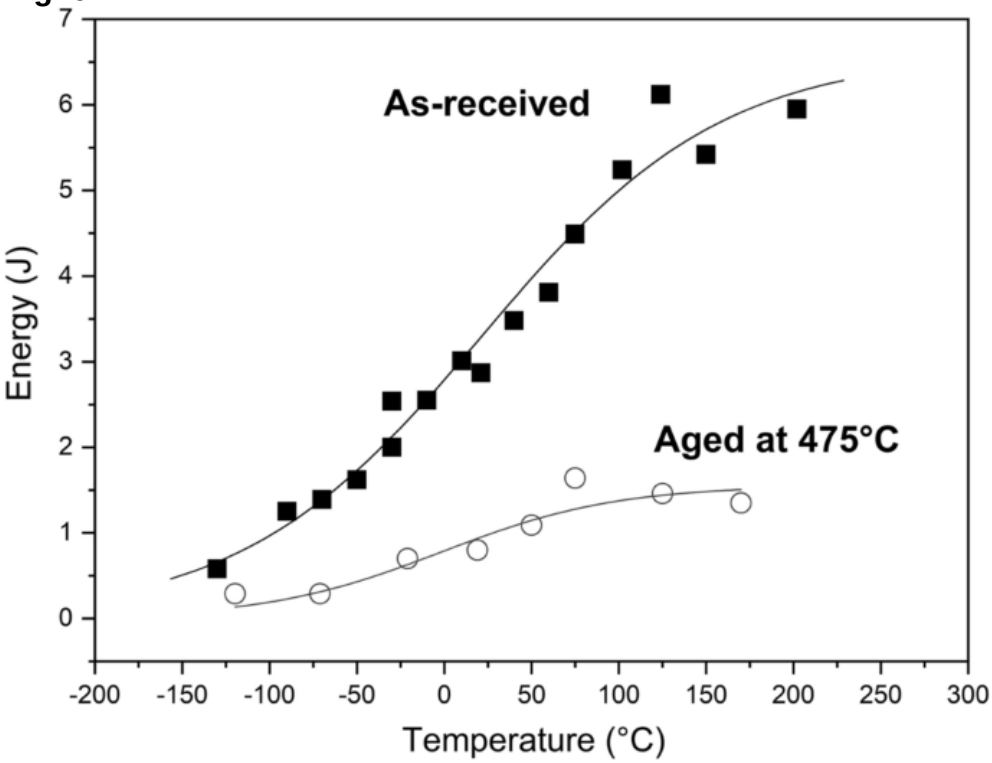

Sub-size Charpy impact test curves obtained for as-received and aged conditions in the Fe–19Cr–5.5Al ODS alloy

This difference in the energy absorbed by the as-received and the aged specimens is bigger with the increase of the testing temperature. The corresponding USE, LSE and DBTT values, extracted from the previous graphic, are listed in Table I.

Table I USE, LSE and DBTT Values Obtained After the Charpy Impact Tests for As-Received and Aged Conditions in the Fe–19Cr–5.5Al ODS Alloy

Sample	USE (J)	LSE (J)	DBTT (°C)
As-received	6.48	0.24	24.64
Aged 475 °C	1.56	0.00	-1.65

The upper shelf energy values achieved (6.48 and 1.56 J for the as-received and aged alloy, respectively) are in the range of those obtained in hipped, hot extruded and other hot rolled ODS alloys.[19,20,21] The lower absorbed energies reached after the aging treatment generate a shift in the DBTT toward a lower value of temperature. Therefore, there is a clear loss of toughness in the steel associated with its embrittlement, that has been reported by other authors as a consequence of the α/α' phase decomposition produced for long time exposures at 475 °C. [10,11,15] After the aging treatment, the Cr-rich α' precipitates formed during the $\alpha–\alpha'$ phase decomposition of the ferritic matrix impede the dislocation motion.[22] Thus, this reduced dislocation mobility involves an embrittlement of the PM2000 alloy, which is manifested through a reduction of the USE. On the other hand, Chao *et al*. mentioned that an increase in the strain rate was responsible for a greater loss of ductility in aged PM2000 tensile specimens.[15] Thus, it is not possible to directly compare the loss of toughness achieved during impact tests with that corresponding to tensile tests since impact tests are performed at a strain rate of six orders of magnitude higher than for tensile tests, and therefore its effect on the loss of toughness and ductility is more evident. The fractographic analysis of the impact specimens after the test, corresponding to TS plane, shows the existence of delaminations in all the samples tested, which are represented by cracks running parallel to the transverse direction of the plate (Figure 7). This delamination phenomenon, also denominated as splitting, was reported by Kimura *et al*. as an intergranular cracking taking place in ultrafine elongated grain structure steels with a strong 〈110〉//RD fiber deformation texture.[23,24] As mentioned above, the 〈110〉//RD texture is also found for the elongated ferritic grains forming the Fe–19Cr–5.5Al ODS steel of the present research (Figure 2). The intergranular cracking is due to the fact that some boundaries between elongated grains act as weak interfaces. This delamination configuration corresponds to the basic geometry that was termed as crack-divider by Kimura *et al.*, in which the weak interfaces were parallel to the longitudinal direction of the impact test bar and the formation of a series of cracks or splits caused a relaxation of the triaxial tension toward a state of biaxial tension, lowering both the DBTT and the USE values.[24] Apart from the existence of elongated grains parallel to the HR direction (LS plane) favoring the grain boundary sliding,[25] the weak interfaces have also been explained as been caused by the increase of the stress in ND due to plastic constraints, together with the presence of second phases, such as Y–Al–Ti nano-oxides, found along grain boundaries in a similar Fe–19Cr–5.5Al ODS manufactured as a tube with a wall thickness of 8 mm.[21]

Fig. 7

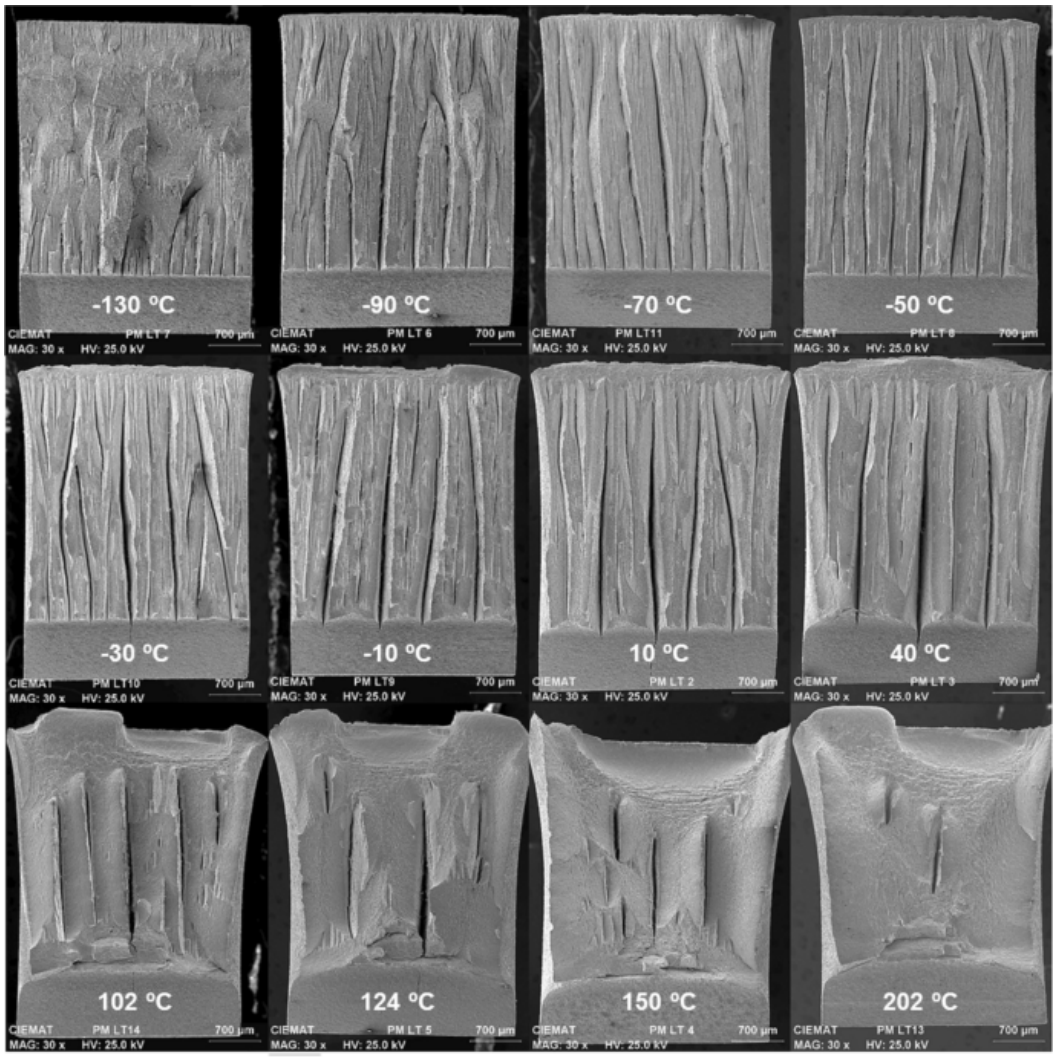

(a) AS-RECEIVED Fe-19Cr-5.5Al ODS

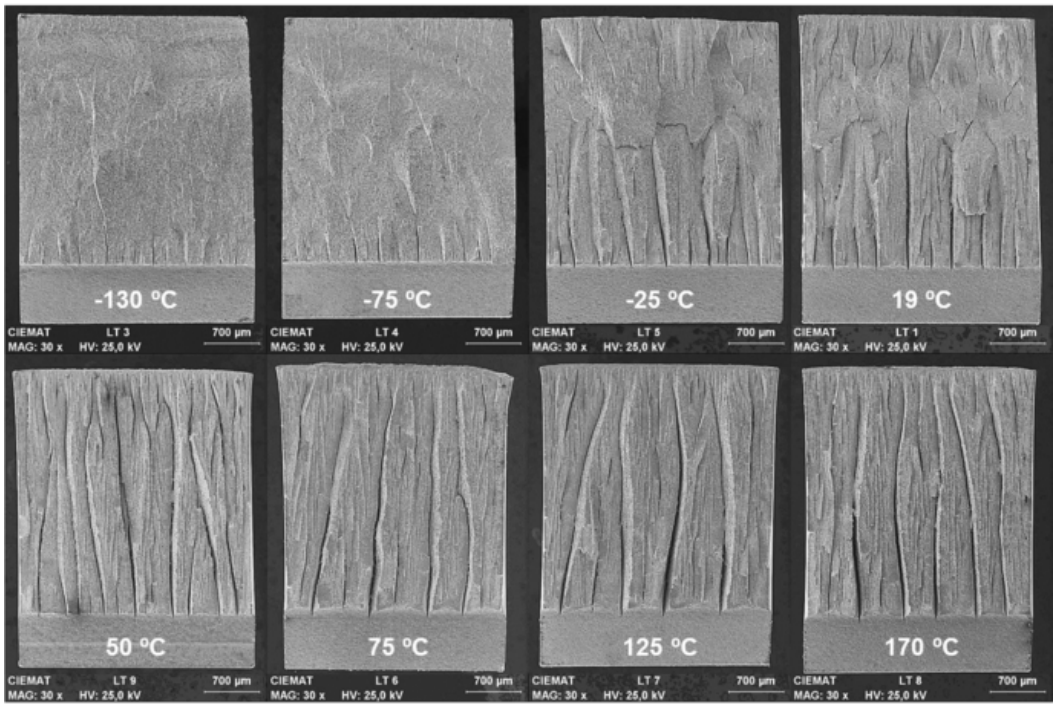

(b) AGED Fe-19Cr-5.5Al ODS

Fractured impact specimens showing a clear splitting in the conditions: (*a*) as-received and (*b*) aged Fe–19Cr–5.5Al ODS alloy

Figure 8 shows schematically the as-received microstructure in the TS plane (EBSD image) and a real micrograph of the TS fractured surface in the KLST-LT Charpy sample

Fig. 8

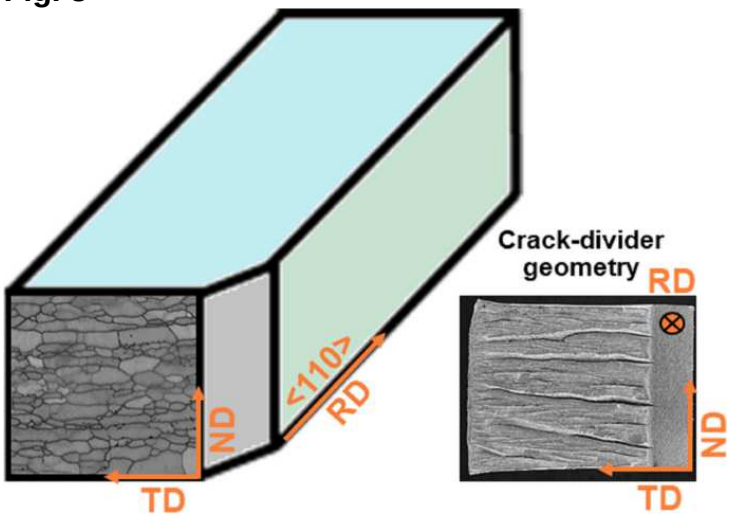

Scheme showing the orientations of the splitting in a fractured KLST-LT Fe–19Cr–5.5Al ODS impact specimen

From this figure, it is clear that the cracks initiated at the notch tip and probably run along TD following weak intergranular ferritic boundaries, as confirmed by Serrano *et al* in a 12 Cr ODS steel following a similar crack-divider configuration.[26] It is remarkable that the space between the parallel delaminations is uniform, and this distance has been reported as reaching a value that is around two times the plastic zone size.[26,27] In the as-received Fe–19Cr–5.5Al ODS, the number of delaminations tends to decrease with the increase of the temperature between − 130 °C and 202 °C, since the behavior of the fracture becomes noticeably more ductile when the test temperature raises (Figure 7(a)). However, in the case of the aged specimens, a high number of delaminations is visible even at a temperature of 170 °C, which is pointing out that the embrittlement is still present at high temperatures (Figure 7(b)). A deeper microstructural analysis of the fractured surfaces of the impact specimens tested at high temperatures, reveals a more ductile fracture, formed mainly by dimples, in the as-received KLST samples than in the aged specimens, where there are more cleavage facets confirming the embrittlement due to the α' formation when aging at 475 °C during 1000 hours (Figure 9). To analyze the embrittlement effect, the hardness was measured in the three different planes of the plate (Table II).

Fig. 9

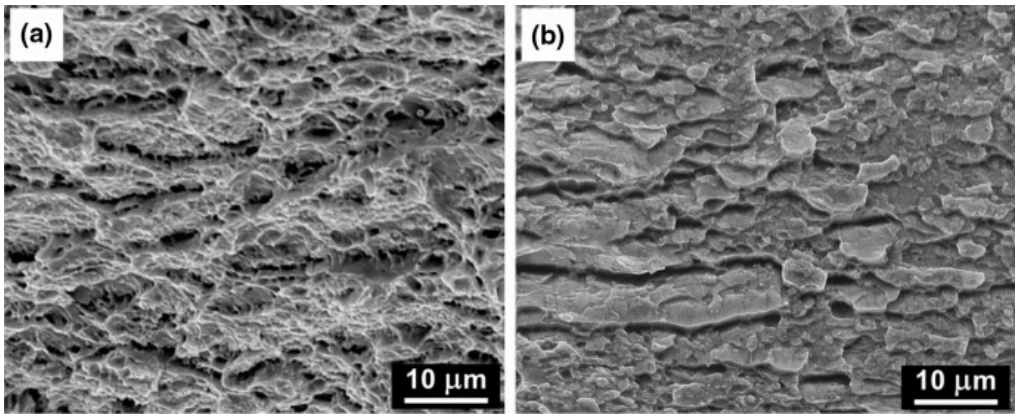

SEM micrographs showing the fractured surface of KLST-LT Fe–19Cr–5.5Al ODS specimens: (*a*) as-received condition tested at 150 °C, (*b*) aged condition tested at 170 °C

Table II Vickers Microhardness in the Three Planes of the Steel Plate (LS, TS and LT) for As-Received and Aged Conditions in the Fe–19Cr–5.5Al ODS Alloy

	HV 0.1	HV0.1
Plane	As-received	Aged 475°C
LS	352±6	403±4
TS	362±5	408±7
LT	362±7	399±4

From the data, it is clear that the different planes have a similar microhardness value for a same condition, as-received or aged. However, as could be expected after the impact test results reported above, the aging treatment has significantly increased the hardness of the ODS alloy. This hardening was explained by Capdevila *et al.* as being caused by a lattice misfit between the emerging α and α' domains and the resulting elastic strain, together with an increment of the elastic modulus due to the α–α' phase separation taking place during the aging treatment at 475 °C.[11]

3.4 Small Punch Tests

The SP test is a technique especially useful for the mechanical characterization in those cases in which the available amount of material is limited and/or the material is highly activated by neutron irradiation.[28] It would be of great relevance to evaluate if this method is able to identify the grade of embrittlement reached after the aging treatment of a hot rolled high-Cr ODS alloy, and the type of fracture involved. The force-displacement curves obtained for the as-received and aged materials at the four testing temperatures are illustrated in Figure 10.

Fig. 10

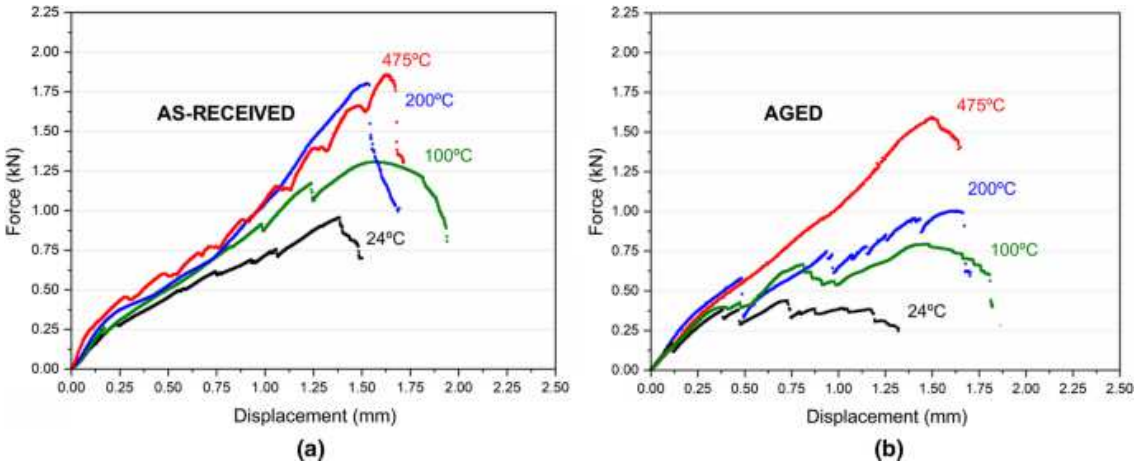

Small punch curves obtained at four different testing temperatures in the Fe–19Cr–5.5Al ODS alloy: (*a*) as-received and (*b*) aged

Although the small punch curves show a decrease of load during the tests for a fixed testing temperature in the aged specimens, it is due to the delamination process. The delamination decreases substantially the loading bearing capability of the disk and thus accelerates the final failure. Actually, the maximum load at the small punch tests cannot be related to the material strength due to the energy absorbed during the subsequent delaminations. However, the deformation values reached (the displacement values shown in Figure 10(b)) seem to diminish slightly with the aging treatment, as it would be expected in an embrittlement process, although a clear effect in the loss of ductility is again hindered by the delamination process suffered by the small punch specimens. Moreover, it is noticeable that the curves present discontinuous load drops, also called pop-ins, that are more frequent and pronounced in the aged than in the as-received steel. These discontinuities are due to the initiation of a crack followed by its arrest. Altstadt *et al*. observed similar discontinuities in the force-displacement curves of a rolled Fe–12Cr ODS steel, due to the formation of delaminations during the SP test.[29] In the present research, the pop-ins tend to diminish with the rise of the temperature as a result of a more ductile behavior of the alloy for both conditions. These findings are perfectly corroborated by the inspection of the fractured SP specimens shown in Figure 11, where it is possible to detect some delaminations that are clearly visible in the as-received condition until a temperature of 100 °C, whereas the aged condition maintains these parallel delaminations up to 200 °C. The appearance of the aged fractured specimens is always more brittle and with lower plastic deformation involved than in the as-received alloy for all the temperatures tested. At 475 °C, both conditions exhibit ruptured SP specimens with circumferential cracks typical from a ductile behavior, although for the aged conditions some small secondary cracks exist, pointing out that some embrittlement is still present at this high temperature.

Fig. 11

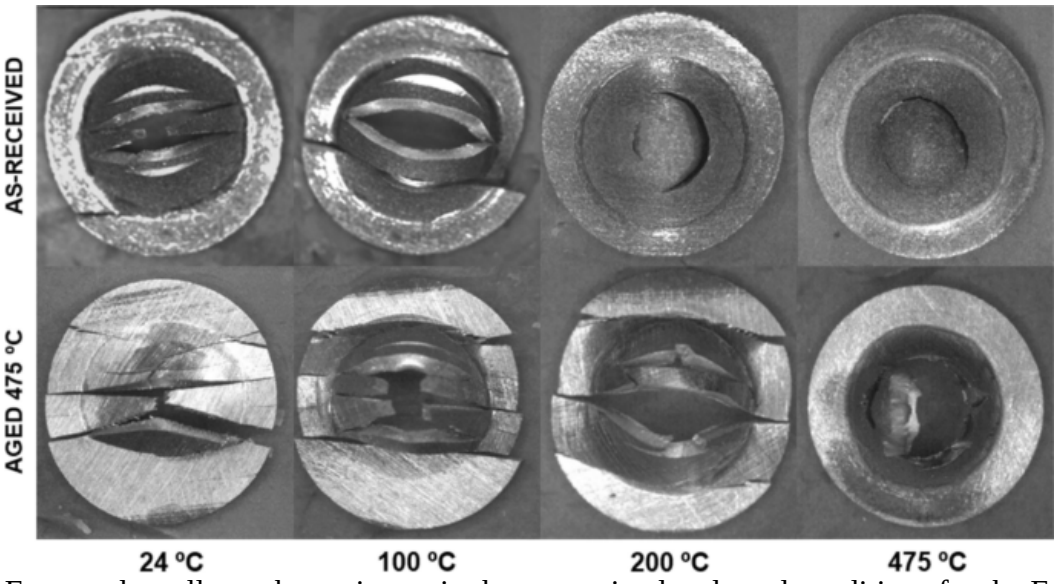

Fractured small punch specimens in the as-received and aged conditions for the Fe–19Cr–5.5Al ODS alloy at four different testing temperatures

3.5 Comparison Between Impact and Small Punch Tests Results

After an exhaustive analysis of the results achieved from the impact and small punch tests, one important outcome obtained is that both mechanical tests are able to detect the embrittlement generated by the aging of the Fe–19Cr–5.5Al ODS alloy at 475 °C during 1000 hours. In the two tests, delaminations are found in the fractured specimens. The delamination or splitting is the consequence of having elongated ferritic grains with a strong texture produced by the hot rolling of the steel plate. This generates weak interfaces between the elongated grains that lead to intergranular cracking, which is observed as parallel cracks in a macroscopic level (Figures 7 and 11). Another relevant finding is that the results of both tests are highly correlated. Thus, the fractographic analysis after the impact and small punch tests clearly shows that the as-received condition exhibit a character mainly ductile at 200 °C, whereas in the aged condition a pronounced brittle behavior is still present at this temperature. Thus, an important key-issue of this research is that the small punch test has been identified as a helpful tool to indicate the grade of embrittlement of a hot rolled steel, which is of particular interest in those cases in which there are small volumes of materials or the activation is elevated.

4 Conclusions

The effect of an isothermal aging at 475 °C for 1000 hours on the mechanical properties of a Fe–19Cr–5.5Al ODS hot rolled steel plate was investigated by means of tensile, impact, microhardness, and small punch tests. This aging temperature was selected since an embrittlement of high-Cr steels has been reported to occur at 475 °C due to the existence of a miscibility gap in the Fe–Cr diagram that leads to a phase separation into a Fe-rich phase (α) and a Cr-rich phase (α'). The main results are summarized as follows:

1. The hot rolled steel plate exhibited a microstructure composed of elongated ferritic grains, with an average size diameter between 0.7 to 0.9 μm, depending on the plane. The ODS had two strong preferential crystallographic orientations

of the grains, being 〈110〉 along the rolling direction and 〈100〉 along the normal direction of the plate.
2. Tensile tests confirmed the increase of both yield strength and ultimate tensile strength at room temperature in the aged specimens. The fracture is also more brittle and formed by some delaminations, which clearly corresponded to an embrittlement of the alloy with the aging treatment.
3. The analysis of the Charpy impact curves after the tests revealed that the aging treatment involved a decrease in the absorbed energy for a given testing temperature. This loss of toughness was greater as the test temperature was increased. Parallel delaminations following a crack-divider configuration were observed in all the fractured LT specimens. This intergranular fracture, also called splitting, followed weak interfaces as a result of having an elongated grain microstructure with a strong 〈110〉//RD texture. The number of delaminations tended to decrease for the as-received material as the testing temperature was raised. However, the aged material presented a great number of delaminations even at 170 °C, possibly due to a significant embrittlement associated with the aging thermal treatment.
4. The microhardness measurements also confirmed the hardening of the ODS material after the aging treatment.
5. The small punch test has demonstrated to be an effective method to identify the grade of embrittlement of a hot rolled steel. The force-displacement curves obtained showed discontinuous load drops, or pop-ins. The pop-ins were more frequent and pronounced in the aged than in the as-received steel, and they are associated with delaminations that were visible in the SP fractured specimens.
6. The results obtained from the tensile, Charpy impact and small punch tests were highly correlated and all techniques were able to identify the embrittlement in the aged ODS alloy.

References

1. S. Ukai and M. Fujiwara: *J. Nucl. Mater.*, 2002, vol. 307–311, pp. 749–57. .
2. K.L. Murty and I. Charit: *J. Nucl. Mater.*, 2008, vol. 383(1–2), pp. 189–95. .
3. I. Hilger, F. Bergner, and T. Weißgärber: *J. Am. Ceram. Soc.*, 2015, vol. 98, pp. 3576–81. .
4. S. Seils, A. Kauffmann, F. Hinrichs, D. Schliephake, T. Boll, M. Heilmaier: *Mater. Sci. Eng. A*, 2020, vol. 786, 139452.
5. H.S. Cho, A. Kimura, S. Ukai, M. Fujiwara*: J. Nucl. Mater.*, 2004, vol. 329–333, part A, pp. 387-91.
6. P. Dubuisson, Y. de Carlan, V. Garat, and M. Blat: *J. Nucl. Mater.*, 2012, vol. 428(1–3), pp. 6–12. .
7. S. Kobayashi and T. Takasugi: *Scr. Mater.*, 2010, vol. 63(11), pp. 1104–7. .
8. M.J. Blackburn and J. Nutting: *Journal of the Iron and Steel Institute.*, 1964, vol. 202, pp. 610–3. .

9. R. Lagneborg: *Acta. Metall.*, 1964, vol. 12, pp. 823–43. .

10. C. Capdevila, M.K. Miller, K.F. Russell, J. Chao, and J.L. González-Carrasco: Mater. *Sci. Eng. A.*, 2008, vol. 490(1–2), pp. 277–88. .

11. C. Capdevila, M.K. Miller, I. Toda, and J. Chao: Mater. *Sci. Eng. A.*, 2010, vol. 527(29–30), pp. 7931–8. .

12. D.A. Terentyev, G. Bonny, and L. Malerba: *Acta Mater.*, 2008, vol. 56(13), pp. 3229–35. .

13. J. Degmová, V. Kršjak, S. Sojak, J. Dekan, M. Petriska, P. Mikula, M.l Kotvas: *J. Nucl. Mater.*, 2021, vol. 547, 152799.

14. B.C. Maji, S. Ukai, N. Oono-Hori: *Mater. Sci. Eng. A*, 2021, vol. 807, 140858.

15. J. Chao, C. Capdevila-Montes, and J.L. González-Carrasco: Mater. *Sci. Eng. A.*, 2009, vol. 515(1–2), pp. 190–8. .

16. C.L. Chen, P. Wang, and G.J. Tatlock: Mater. *High Temp.*, 2009, vol. 26(3), pp. 299–303. .

17. ASTM E3205-20, Standard Test Method for Small Punch Testing of Metallic Materials, ASTM International, West Conshohocken, PA, 2020.

18. M. Dahms and H.J. Bunge: *J. Appl. Cryst.*, 1989, vol. 22, pp. 439–47. .

19. R. Lindau, A. Möslang, M. Schirra, P. Schlossmacher, M. Klimenkov: *J. Nucl. M.ter.*, 2002, vol. 307-311, part 1, pp. 769-72.

20. A. García-Junceda, M. Hernández-Mayoral, and M. Serrano: *Mater. Sci. Eng. A.*, 2012, vol. 556, pp. 696–703. .

21. J. Chao, C. Capdevila, M. Serrano, A. García-Junceda, J.A. Jiménez, G. Pimentel, and E. Urones-Garrote: Metall. *Mater. Trans. A.*, 2013, vol. 44(8), pp. 4581–94. .

22. Z. Száraz, P. Hähner, J. Stráská, and S. Ripplinger: *Mater. Sci. Eng. A.*, 2017, vol. 700, pp. 425–37. .

23. Y. Kimura, T. Inoue, F. Yin, O. Sitdikov, and K. Tsuzaki: *Scr. Mater.*, 2007, vol. 57(6), pp. 465–8. .

24. Y. Kimura, T. Inoue, F. Yin, and K. Tsuzaki: *ISIJ Int.*, 2010, vol. 50(1), pp. 152–61. .

25. H. Okada, S. Ukai, and M. Inoue: *J. Nucl. Sci. Technol.*, 1996, vol. 33(12), pp. 936–43. .

26. M. Serrano, A. García-Junceda, R. Hernández, and M.H. Mayoral: *Mater. Sci. Technol.*, 2014, vol. 30(13b), pp. 1664–8. .

27. S. Kalyanam, A.J. Beaudoin, R.H. Dodds, F. Barlat: *Eng. Fracture Mechanics*, 2009, vol. 76(14), pp. 2174-91.

28. E. Altstadt, H.E. Ge, V. Kuksenko, M. Serrano, M. Houska, M. Lasan, M. Bruchhausen, J.-M. Lapetite, and Y. Dai: *J. Nucl. Mater.*, 2016, vol. 472, pp. 186–95. .

29. E. Altstadt, M. Serrano, M. Houska, and A. García-Junceda: *Mater. Sci. Eng. A.*, 2016, vol. 654, pp. 309–16. .

Acknowledgments

Authors want to acknowledge Ferro-Genesys project funded by MINECO under National I+D+I program MAT2013-47460-C5-4-P. Authors would like to express their sincere gratitude to Daniel Plaza for the help received during the impact tests and to Fernando Plaza for the drawing of the tensile test specimen shown in Figure 1 of this paper.

Conflict of interest

The authors declare that they have no conflict of interest.